ACS OMEGA

http://pubs.acs.org/journal/acsodf

Article

Direct Conversion of Syngas to Light Olefins over a $ZnCrO_x$ + H-SSZ-13 Bifunctional Catalyst

Yuxuan Huang, Hongfang Ma, Zhiqiang Xu, Weixin Qian, Haitao Zhang, and Weiyong Ying*

Cite This: *ACS Omega* 2021, 6, 10953−10962

Read Online

ACCESS | Metrics & More | Article Recommendations | Supporting Information

ABSTRACT: In recent years, bifunctional catalysts for the syngas-to-olefins (STO) reaction via the oxide−zeolite (OX−ZEO) strategy has been intensively investigated. However, the bifunctional catalyst containing H-SSZ-13 with a 100% H^+-exchanging degree for the STO reaction has not been developed because of the high selectivity to paraffin. Here, we report a $ZnCrO_x$ + H−SSZ-13 bifunctional catalyst, which contains the submicron H−SSZ-13 with adequate acidic strength. Light olefins in hydrocarbon reached 70.8% at a CO conversion of 20.9% over the $ZnCrO_x$ + H−SSZ-13(23S) bifunctional catalyst at 653 K, 1.0 MPa, and GHSV = 6000 $mL \cdot g^{-1} \cdot h^{-1}$ after 800 min of STO reaction. The effect of CO and H_2 on the C−C coupling was discussed by carrying out the methanol-to-olefins (MTO) reaction under a similar atmosphere as that of the STO reaction. H_2 and CO should play a more dominant role than the conventional hydrogen transfer reaction on the undesired high selectivity of paraffins. These findings provide new insight into the design of the bifunctional catalyst for the STO process via the OX−ZEO strategy.

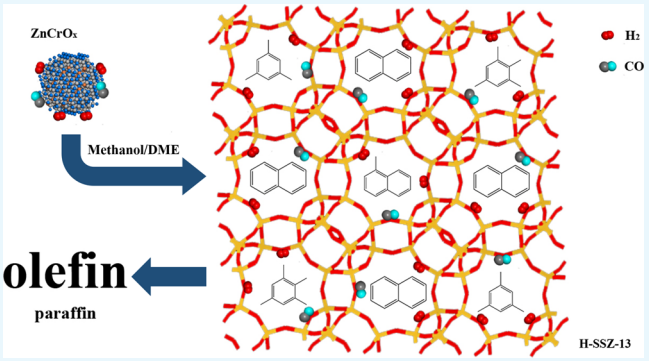

1. INTRODUCTION

Light olefins (C_2−C_4) are the key building blocks in the petrochemical industry with great demand. Syngas, consisting of CO and H_2, can be derived from not only coal and natural gas but also biomass, which makes it more sustainable than crude oil. Thus, the direct conversion of syngas to light olefins (STO) is an attractive process to realize non-oil-based light olefin production, which has been researched for decades.[1,2] In the past 5 years, considerable research efforts have been devoted to the STO process via the oxide−zeolite (OX−ZEO) strategy. CO was activated over the metal oxide, and C−C coupling proceeded over the acid sites in the zeolite. Several kinds of metal oxides have been utilized in the bifunctional catalysts, such as $ZnCrO_x$,[3−7] ZrO_2−ZnO,[8] $ZnAlO_x$,[9] ZnO,[10] MnO_x,[11] and Zr−In_2O_3.[12] SAPO-34, a silicoaluminophosphate zeotype with a chabazite (CHA) structure,[13] is the most popular zeotype used in the bifunctional catalyst for the STO process[4,5,8−12] and responsible for its excellent performance in the methanol-to-olefins (MTO) process.[14−16] Other kinds of zeolites/zeotypes have been used in the bifunctional catalyst for the STO process as well, such as mordenite,[6] AlPO-18,[7] and SSZ-13,[17] but these zeolites/zeotypes received less attention than SAPO-34. The intermediate between CO activation and C−C coupling remained controversial since the first time when the OX−ZEO strategy was presented.[5,8] Several works supported ketene as the intermediate of the STO reaction,[5,6,18] while considerable research studies in the recent years have speculated that methanol plays a greater role than ketene during the STO reaction.[7−9,17,19]

SSZ-13, the aluminosilicate analogue of SAPO-34, is a kind of zeolite with a CHA structure.[20] Cu ion-exchanged SSZ-13 zeolite (Cu−SSZ-13) is an important catalyst in the selective catalytic reduction of NO_x with the NH_3 (NH_3−SCR) process.[21−23] The ability of the proton type of SSZ-13 (H−SSZ-13) in the MTO process has been discovered,[24−26] which makes H−SSZ-13 the potential zeolite in the bifunctional catalyst for the STO process since the STO process via the OX−ZEO strategy can be understood as the combination of the syngas-to-dimethyl ether (STD) process and the MTO process.[9]

Liu et al. utilized SSZ-13 as the zeolite in the bifunctional catalyst for the STO process for the first time. H−Na−SSZ-13 with a 45% H^+-exchanging degree (SSZ-13-45H) was mixed with Zn−ZrO_2, forming the bifunctional catalyst for the STO process. However, the bifunctional catalyst containing the fully H^+-exchanging zeolite (H−SSZ-13 with a 100% H^+-exchanging degree) only showed a light olefins selectivity of less than 10%

Received: February 10, 2021
Accepted: April 8, 2021
Published: April 19, 2021

in the STO reaction, while C_2-C_4 paraffins were the dominant products.[17] The bifunctional catalyst for the STO process containing H−SSZ-13 has not been successfully developed up to now because of the excessive formation of paraffins. Despite the academic interest, the utilization of H−SSZ-13 in the bifunctional catalyst should be more accessible and repeatable in its potential industrial application.

Hydrogen transfer reaction is regarded as the source of paraffin formation during the MTO process. Since the conventional MTO process is operated under H_2-free circumstances, the formation of paraffins would concurrently lead to the formation of hydrogen-deficient species and subsequently results in the formation of aromatics.[27,28] However, syngas consists of CO and H_2, which means that the MTO reaction during the STO process is operated under a H_2-rich atmosphere. Some experimental and theoretical studies have revealed that olefin hydrogenation would happen over the acid sites of zeolites.[29,30] Zhao et al. pointed out that olefin hydrogenation might be considered as the source of paraffin formation during the MTO process operated under the H_2-rich atmosphere.[19]

Herein, the bifunctional catalyst consisting of $ZnCrO_x$ and H−SSZ-13 was prepared for the STO process via the OX−ZEO strategy. Light olefins were the dominant products over the bifunctional catalyst containing H−SSZ-13 with a 100% H^+-exchanging degree. XRD, inductively coupled plasma-optical emission spectrometry, SEM, Ar physisorption, and NH_3−temperature-programmed desorption were used to characterize the structure and acidic property of the catalyst. The MTO tests under the atmospheric He, high-pressure H_2, and high-pressure syngas were performed to reveal the MTO performance of H−SSZ-13 under the pseudo-reaction condition in the STO process. The carbonaceous species were investigated by GC−MS and TG.

2. RESULTS AND DISCUSSION

2.1. Structure and Acidic Property. As shown in Figure 1, although the preparation method and the Si/Al ratio were different, all calcined samples exhibited the CHA structure. However, the different preparation methods and the Si/Al ratio led to a completely different morphology of the zeolite particles. Figure 2 displays that the particles of H−SSZ-13 prepared by the conventional method tended to aggregate as the Si/Al ratio increased. The particle size of H−SSZ-13 (12C) was 250−500 nm, and no distinct aggregation was observed (Figure 2E). The particle size of H−SSZ-13 (19C) increased to 3−5 μm (Figure 2B), which displayed a rough surface. From the picture taken under higher magnification (Figure 2F), it can be found that the micrometer-scaled particles consisted of submicron particles which had a similar size to HSSZ-13 (12C). Therefore, the micrometer-scaled size of H−SSZ-13 (19C) ought to result from the aggregation of the submicron particles. Along with the further increase of the Si/Al ratio in H−SSZ-13(C), the particle size kept growing to 6−10 μm (Figure 2C,D). There were very few individual submicron particles, while submicron embossing on the surface of the micrometer-scaled particles could be observed (Figure 2G,H). Meanwhile, the H−SSZ-13 zeolites prepared by the seed-assisted hydrothermal synthesis consisted of the submicron particles, and the particles could be distinguished from each other even at a high Si/Al ratio (Figure 2I−L).

Table S2 shows the textural properties of H−SSZ-13.[31] The external surface of H−SSZ-13(C) decreased as the Si/Al ratio increased, which should be owed to the large particle size of H−SSZ-13(C) with the high Si/Al ratio. H−SSZ-13 (12C) displayed a similar external surface area as H−SSZ-13(S) since it consisted of submicron particles, although it was prepared by the conventional hydrothermal synthesis. The high external surface area of the zeolite implied that the abundant outer cages were exposed, which should facilitate the diffusion of the reactant and products.

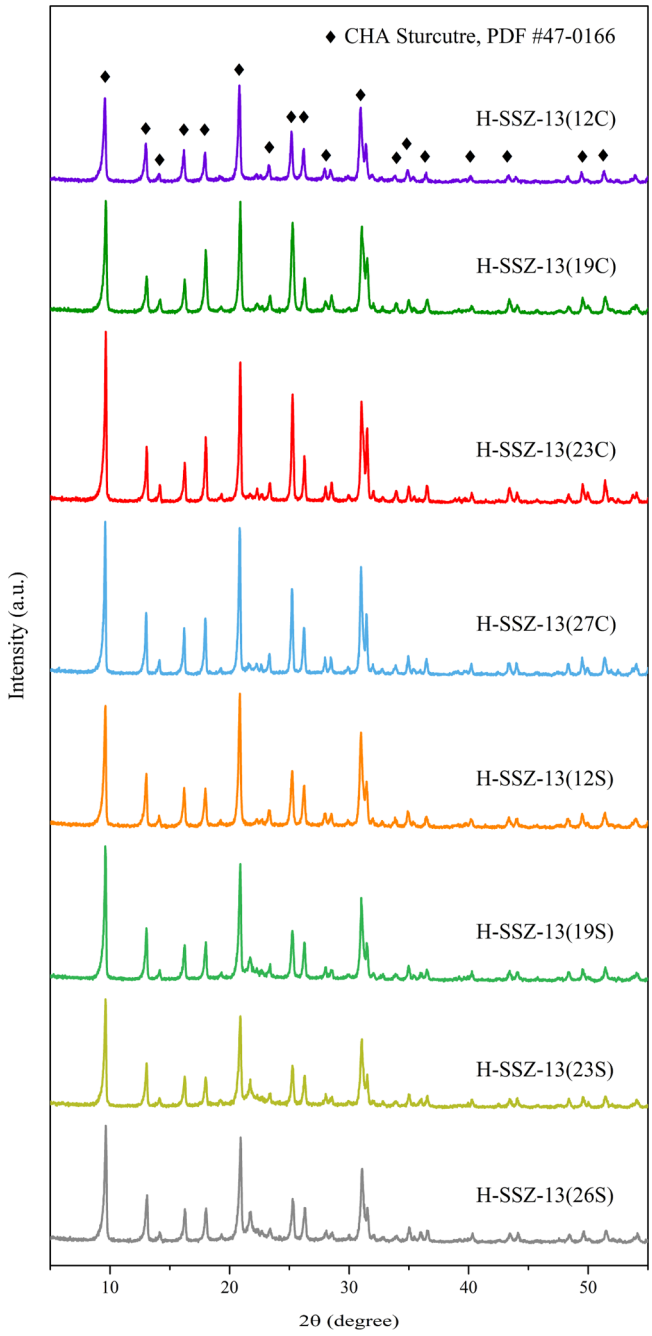

Figure 1. XRD patterns of H−SSZ-13.

The NH_3−TPD profiles showed that all H−SSZ-13 exhibited two major desorption peaks (Figure 3). The high-temperature peaks, corresponding to the strong-acid sites,[32] located in the range of 650−700 K, which were much higher than the peaks for H−SAPO-34 (600−630 K).[4] Thus, the acid strength of H−SSZ-13 was much stronger than that of H−SAPO-34, which resulted in the low selectivity of light olefins

https://doi.org/10.1021/acsomega.1c00751
ACS Omega 2021, 6, 10953−10962

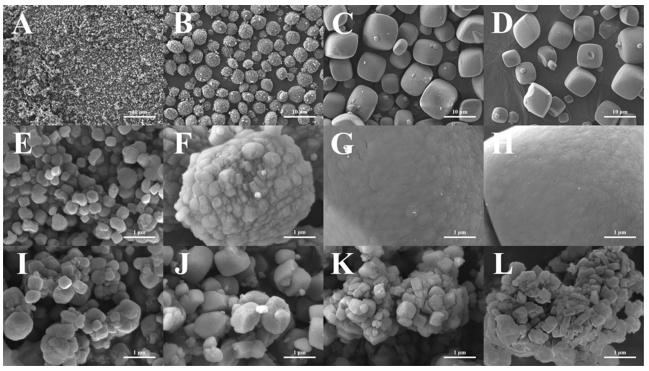

Figure 2. SEM pictures of H−SSZ-13. (A) H−SSZ-13 (12C), 5000*x*; (B) H−SSZ-13 (19C), 5000*x*; (C) H−SSZ-13 (23C), 5000*x*; (D) H−SSZ-13 (27C), 5000*x*; (E) H−SSZ-13 (12C), 50,000*x*; (F) H-SSZ-13 (19C), 50,000*x*; (G) H−SSZ-13 (23C), 50,000*x*; (H) H−SSZ-13 (27C), 50,000*x*; (I) H−SSZ-13(12S), 50,000*x*; (J) H−SSZ-13(19S), 50,000*x*; (K) H−SSZ-13(23S), 50,000*x*; and (L) H−SSZ-13(26S), 50,000*x*.

over the bifunctional catalysts containing H−SSZ-13 in the previous work.[17] The acid strength became weaker along with the increasing Si/Al ratio in both H−SSZ-13(C) and H−SSZ-13(S), but the high-Si/Al-ratio H−SSZ-13(S) showed a weaker strong-acid site than the H−SSZ-13(C) with the similar Si/Al ratio.

2.2. Catalytic Performance of the MTO Reaction and the Carbonaceous Species. Herein, the MTO reaction over H−SSZ-13 under atmospheric He, 0.6 MPa H_2, and 1.0 MPa syngas were carried out. The MTO reaction under 0.6 MPa H_2 was aimed to simulate the same H_2 partial pressure during the STO reaction and eliminated the influence of CO (The STO reaction was carried out under 1.0 MPa syngas containing 60% H_2, which meant that the H_2 partial pressure during the STO reaction was 0.6 MPa). The MTO reaction under 1.0 MPa syngas was carried out to imitate the same atmosphere during the STO reaction. H−SSZ-13(12S), H−SSZ-13 (12C), H−SSZ-13(23S), and H−SSZ-13 (23C) were selected to be compared.

Table 1 shows that methanol conversion over all tested H-SSZ-13 was higher than 99.7% after 800 min of MTO reaction, which meant the absence of deactivation. The selectivity of C_2−C_3 paraffins was lower than 2.5% among all H−SSZ-13 in the He−MTO reaction, which manifested that the contribution of the hydrogen transfer reaction to the high paraffins selectivity was very limited. As for the MTO reaction proceeding under 0.6 MPa H_2, there were two remarkable phenomena. The C_2−C_3 olefins selectivity and C_2−C_3 olefin/paraffin ratio (o/p) dropped dramatically, while H−SSZ-13 with a higher Si/Al ratio displayed a higher C_2−C_3 olefins selectivity and C_2−C_3 o/p, which should be related to the weaker acid strength. Meanwhile, the selectivity of CH_4 increased unexpectedly. When 1.0 MPa syngas was inducted (H_2 partial pressure in the Syngas−MTO and the H_2−MTO were both 0.6 MPa), the C_2−C_3 olefins selectivity and C_2−C_3 o/p increased, while the selectivity of CH_4 decreased. The selectivity of C_{4+} products also increased, which implied that the product distribution shifted to heavier products.

There were two speculations for the high C_2−C_3 paraffin selectivity of the MTO reaction under the H_2-rich atmosphere. The first one was that the hydrogen transfer reaction was enhanced under high-pressure H_2. The second one was that

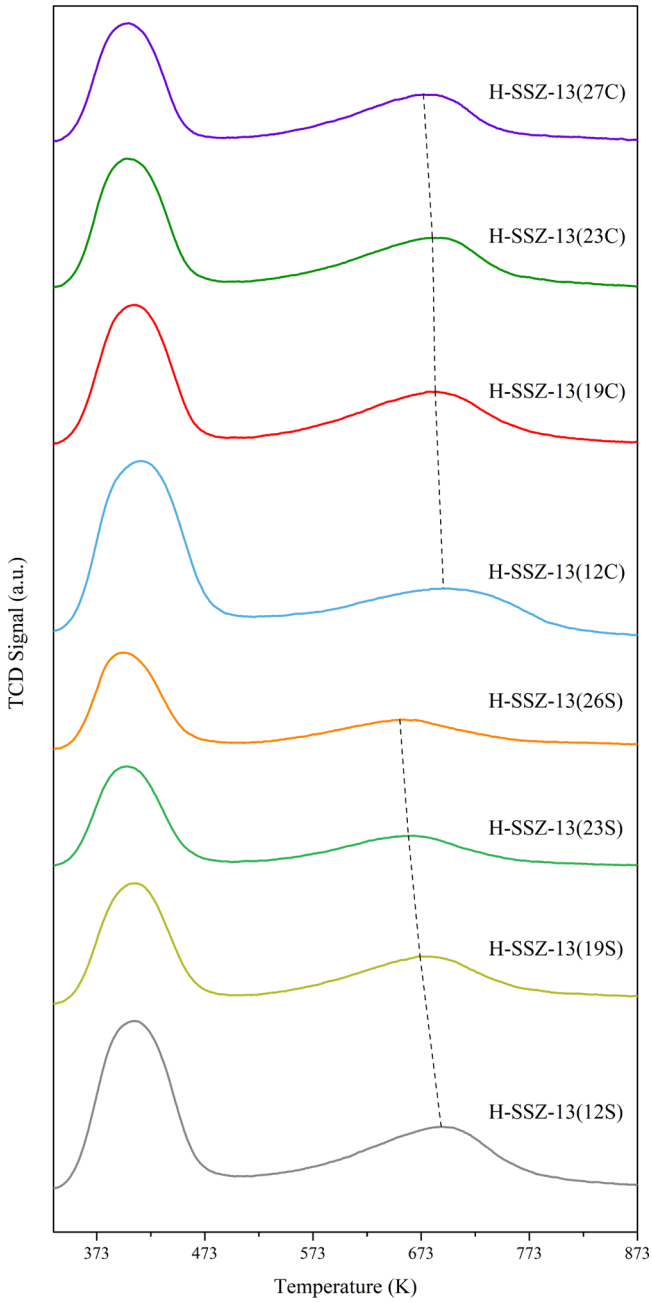

Figure 3. NH_3−TPD profiles of H−SSZ-13.

hydrogenation should play a more dominant role than the conventional hydrogen transfer reaction on the undesired high selectivity of paraffins.

It has been clarified that aromatics would be generated inevitably during the hydrogen transfer reaction as long as the paraffin formation occurs since the hydrogen molecule cannot participate in the hydrogen transfer reaction directly.[27] As shown in Table 1, the C_2−C_3 o/p of all tested H−SSZ-13 in He−MTO (TOS = 800 min) was higher than 37, which means that the hydrogen transfer reaction did exist but its contribution to paraffin formation under the H_2-free atmosphere was very limited. If the hydrogen transfer reaction was enhanced under high-pressure H_2, the formation of the aromatic should also be facilitated. However, Figure 4 shows that the carbonaceous species retained in the spent H−SSZ-13 after 800 min of the MTO reaction under 0.6 MPa H_2 were

https://doi.org/10.1021/acsomega.1c00751
ACS Omega 2021, 6, 10953−10962

Table 1. Catalytic Performance of MTO Reaction Over H−SSZ-13 under Different Atmospheres[a]

atmosphere	zeolite	methanol conversion (%)	hydrocarbon distribution (%)				
			CH_4	$C_{2-3}^{=}$	C_{2-3}^{o}	C_{4+}	C_{2-3} o/p
He−MTO	H−SSZ-13 (12C)	100.0	2.5	85.5	1.0	11.1	85.0
	H−SSZ-13 (23C)	99.8	2.0	83.7	2.2	12.1	37.3
	H−SSZ-13(12S)	100.0	2.4	84.0	1.8	11.8	46.2
	H−SSZ-13(23S)	99.9	2.4	84.0	0.8	12.9	107.1
H_2−MTO	H−SSZ-13 (12C)	100.0	20.3	12.2	55.6	12.0	0.2
	H−SSZ-13 (23C)	100.0	17.7	36.1	27.4	18.9	1.3
	H−SSZ-13(12S)	100.0	18.7	21.9	43.7	15.8	0.5
	H−SSZ-13(23S)	100.0	17.6	31.3	30.6	20.5	1.0
Syngas−MTO	H−SSZ-13 (12C)	100.0	9.0	37.9	29.0	24.0	1.3
	H−SSZ-13 (23C)	100.0	7.3	55.1	15.2	22.5	3.6
	H−SSZ-13(12S)	99.9	7.4	46.6	22.3	23.8	2.1
	H−SSZ-13(23S)	99.9	6.8	54.3	12.2	26.7	4.4

[a]Reaction conditions: 653 K, WHSV = 0.77 $g{\cdot}g^{-1}{\cdot}h^{-1}$, and TOS = 800 min. He−MTO: atmosphere 99% He−1% N_2; H_2−MTO: 0.63 MPa 95% H_2−5% N_2, which provided the H_2 partial pressure of 0.60 MPa; Syngas−MTO: 1.00 MPa 60% H_2−30% CO−10% N_2.

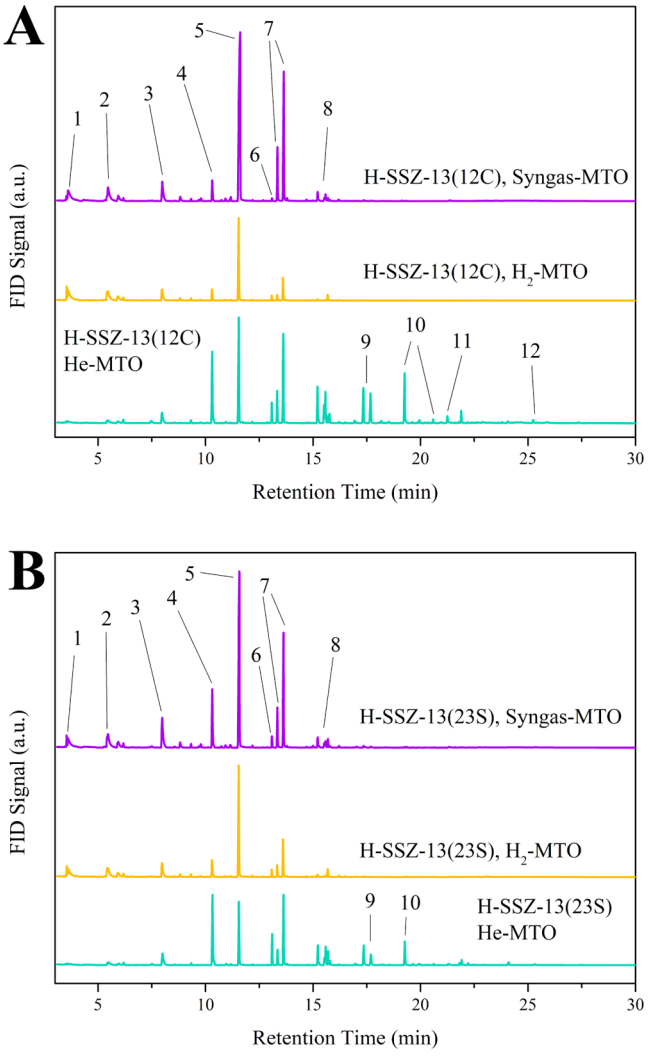

Figure 4. GC−MS results of the soluble carbonaceous species retained in H−SSZ-13 after 800 min of MTO reaction. (A) H−SSZ-13 (12C) and (B) H−SSZ-13(23S). 1-Toluene; 2-xylenes; 3-trimethyl−benzenes; 4-tetramethyl−benzenes; 5-naphthalenes; 6-pentamethyl−benzenes; 7-methyl−naphthalenes; 8-dimethyl−naphthalenes; 9-trimethyl−naphthalenes; 10-tetramethyl−naphthalenes; 11-pyrene; and 12-methyl−pyrene.

lighter than those in the spent H−SSZ-13 after the MTO reaction under He, which implied that the formation of the aromatic was inhibited. What is more, the TG results showed that the amount of the total carbonaceous species retained in the spent H−SSZ-13 after the H_2−MTO was less than those retained in the spent H−SSZ-13 after the He-MTO (Figure 5). According to the previous research on the cofeeding of H_2 during the MTO process,[19] although H_2 could retard the conversion of light aromatics (methylbenzenes and methylnaphthalenes) to heavy aromatics, it could not eliminate the generated light aromatics. Thus, the introduction of 0.6 MPa H_2 during the MTO reaction not only prompted to lighten the retained carbonaceous species distribution but also inhibited the carbonaceous species generation quantitatively. Aromatics formation was inevitable during the hydrogen transfer reaction; thus, the restriction to the carbonaceous species generation should indicate that the hydrogen transfer reaction was restricted as well. Therefore, the hydrogen transfer reaction should not be enhanced during the MTO process under the high-pressure H_2, which meant that it should not be the dominant factor resulting in the high selectivity of C_2−C_3 paraffins in the MTO reaction under the H_2-rich atmosphere and the high selectivity of paraffins in the STO reaction.

As for the second speculation, hydrogenation should play a more dominant role than the conventional hydrogen transfer reaction on the undesired high selectivity of paraffins. The undesired C_2−C_3 paraffins should not be formed by the hydrogenation of C_2−C_3 olefins in the gas phase since the C_2−C_3 o/p increased as the Si/Al ratio increased, which meant that H−SSZ-13 containing stronger-acid sites tended to generate more paraffins under the H_2-rich atmosphere. The undesired C_2−C_3 paraffins might be mainly formed via hydrogenation over the strong-acid sites in the zeolite but not as the result of the conventional hydrogen transfer reaction.

Furthermore, compared with H_2−MTO, the C_2−C_3 olefins selectivity and C_2−C_3 o/p increased in the Syngas−MTO despite the same H_2 partial pressure, suggesting that CO participated in the MTO reaction as well. Figure 4 shows that the proportion of methylbenzenes and methylnaphthalenes in the retained carbonaceous species increased after CO was inducted, although naphthalene was still the dominant species. The TG profiles proved that more carbonaceous species were retained in the zeolite after the Syngas−MTO, compared to H_2−MTO (Figure 5). CO altered the distribution of the

https://doi.org/10.1021/acsomega.1c00751
ACS Omega 2021, 6, 10953−10962

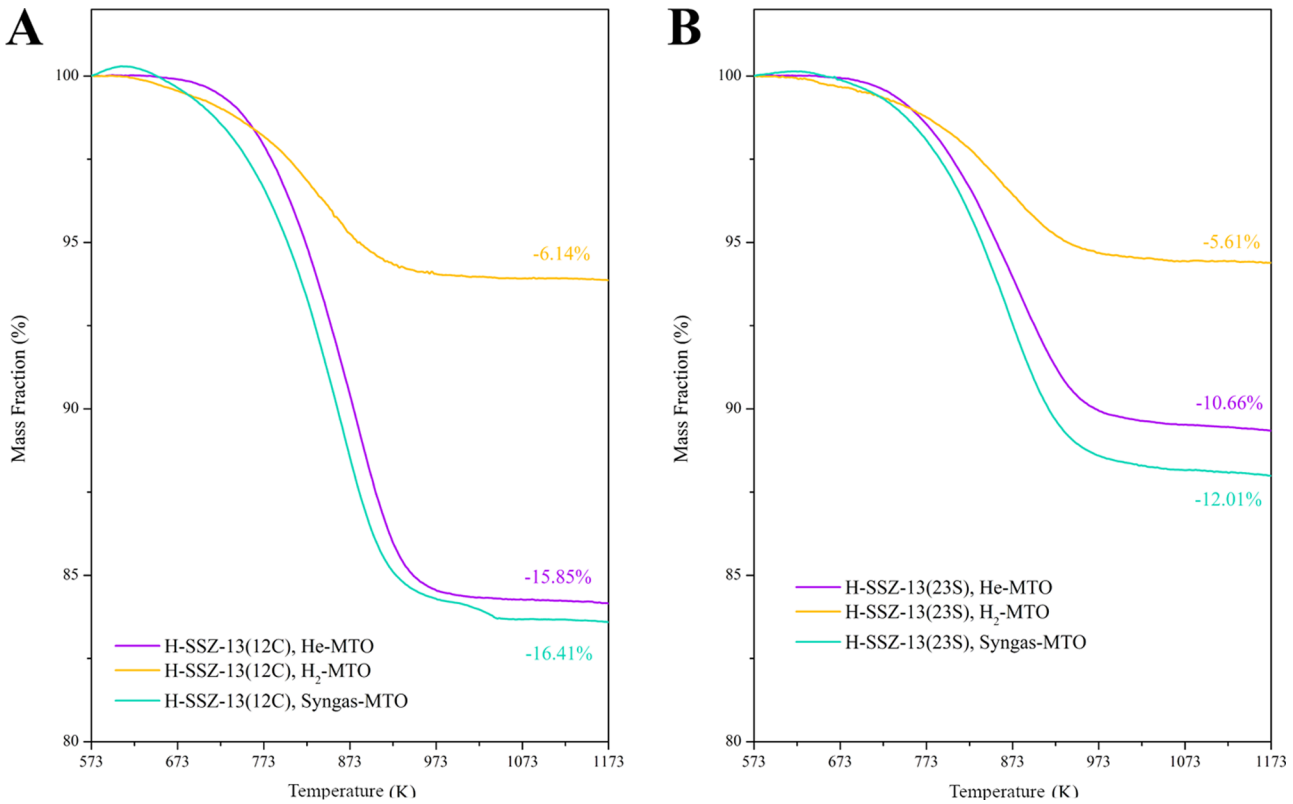

Figure 5. TG results of the spent H−SSZ-13 after 800 min of MTO reaction. The base was set at 573 K. (A) H−SSZ-13 (12C) and (B) H−SSZ-13(23S).

retained carbonaceous species in the zeolite pores, consequently affecting product selectivity in the MTO reaction under the H_2-rich atmosphere.

The role of CO and H_2 in the MTO reaction used to be neglected since they were not able to react with each other directly over the MTO catalyst, and neither CO nor H_2 would be fed intentionally during the conventional MTO process. However, the STO process via the OX−ZEO strategy contains the MTO reaction under the H_2-rich and CO-rich conditions. CO and H_2 could alter the retained carbonaceous species and the product distribution during the MTO process, consequently determining the product selectivity of the STO process. Thus, the influence of CO and H_2 over the zeolite should also be considered in the design of the bifunctional catalyst for the STO process.

2.3. Catalytic Performance of the STO Reaction and the Carbonaceous Species. GC−MS results illustrated the soluble carbonaceous species retained in the bifunctional catalyst after 800 min of the STO reaction. Naphthalene was the major carbonaceous species retained in the spent $ZnCrO_x$ + H−SSZ-13(12S), while tetramethyl−benzenes, methyl−naphthalenes, and trimethyl−benzenes were the secondary species (Figure 6A). As the Si/Al ratio increased in H−SSZ-13(S), tetramethyl−benzenes and trimethyl−benzenes occupied the larger share, while the proportion of naphthalenes and methyl−naphthalenes decreased gradually. Since the particle sizes of H−SSZ-13(S) with different Si/Al ratios were similar to each other, the change in the retained carbonaceous species distribution could only be attributed to the different acidic properties. It can be concluded that the benzene-based species tended to be formed in the submicron H−SSZ-13 with the weaker acid strength, while the naphthalene-based species were more likely to be generated in the submicron H−SSZ-13 with the stronger acid strength.

As for $ZnCrO_x$ + H−SSZ-13(C), naphthalene was the major retained carbonaceous species for all of the samples (Figure 6B). Compared with $ZnCrO_x$ + H−SSZ-13 (12C), the carbonaceous species distribution once showed the tendency of shifting to tetramethyl−benzenes in $ZnCrO_x$ + H−SSZ-13 (19C), but the proportion of naphthalene kept growing as the Si/Al ratio increased further. The tendency of the growth of tetramethyl−benzenes in $ZnCrO_x$ + H−SSZ-13 (19C) could be explained by the weaker acid strength, as previously mentioned. However, the $ZnCrO_x$ + H−SSZ-13(C) bifunctional catalyst with the weaker acid strength showed a higher proportion of naphthalene-based species after the STO reaction, which should be owed to the larger particle size. The zeolite with larger particle size possessed fewer outer cages. The carbonaceous species formed in the outer cages would hinder the diffusion of the reactant and products and prevent the utilization of the inner cages during the reaction. At the same time, the heavier species was generated.[33,34] The diffusion restriction decreased the MTO activity of H−SSZ-13(C) with a high Si/Al ratio, subsequently weakened the thermodynamic driving force between the CO activation and C−C coupling, and finally resulted in a decrease in CO conversion in the STO reaction over the bifunctional catalyst containing H−SSZ-13(C) with a high Si/Al ratio.

As shown in Table 2, the main products over $ZnCrO_x$ + H−SSZ-13 (12C) during the STO reaction were C_2−C_4 paraffins. Along with the growth of the Si/Al ratio, the light olefins selectivity and C_2−C_4 o/p increased simultaneously, which should be owed to the gradually weaker acidic strength of the zeolite. However, the CO conversion dropped from 19.6 to

https://doi.org/10.1021/acsomega.1c00751
ACS Omega 2021, 6, 10953−10962

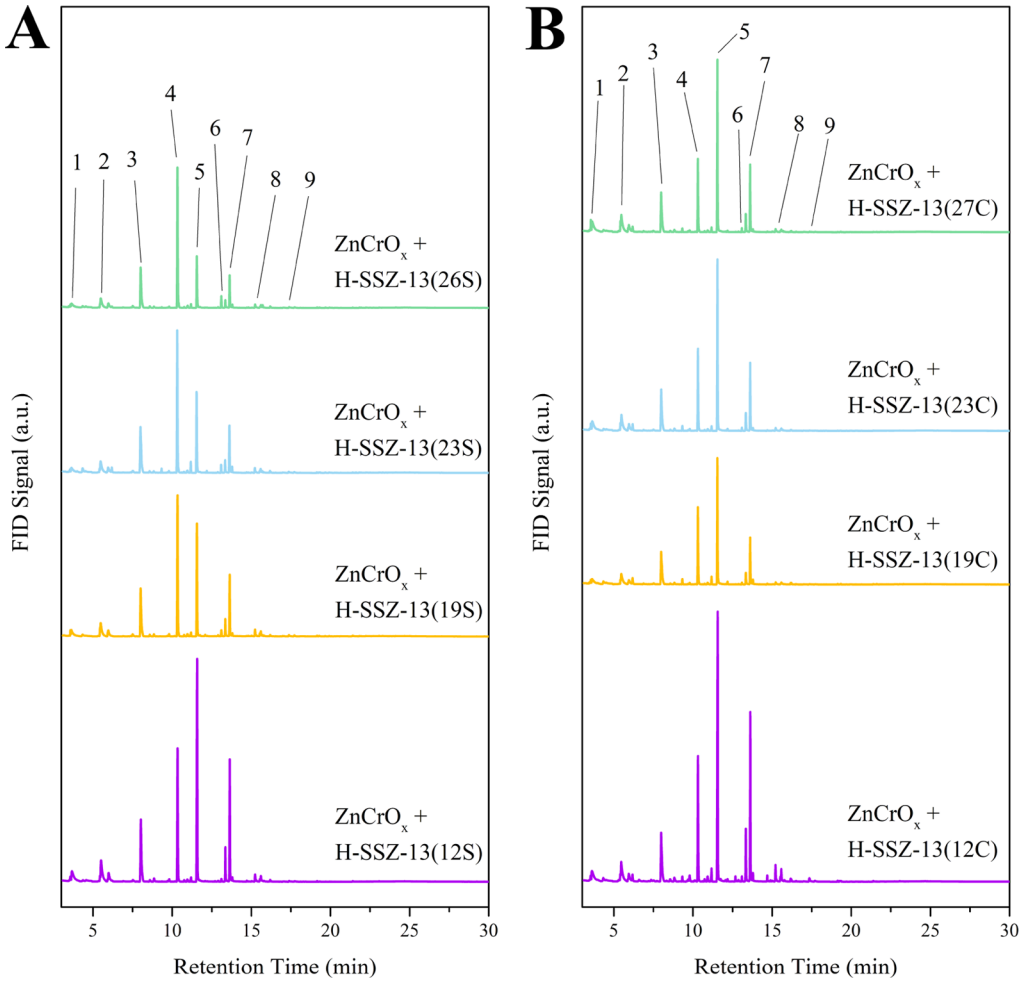

Figure 6. GC−MS results of the soluble carbonaceous species retained in the bifunctional catalysts after 800 min of STO reaction. (A) $ZnCrO_x$ + H−SSZ-13(S) and (B) $ZnCrO_x$ + H−SSZ-13(C). 1-Toluene; 2-xylenes; 3-trimethyl−benzenes; 4-tetramethyl−benzenes; 5-naphthalenes; 6-pentamethyl−benzenes; 7-methyl−naphthalenes; 8-dimethyl−naphthalenes; and 9-trimethyl−naphthalenes.

Table 2. Catalytic Performance of the STO Reaction Over the $ZnCrO_x$ + H−SSZ-13 Bifunctional Catalyst[a]

		hydrocarbon distribution (%)						
zeolite in bifunctional catalyst	CO conversion (%)	CH_4	$C_{2-4}^{=}$	C_{2-4}^{o}	C_{5+}	CO_2 selectivity (%)	C_{2-4} o/p	light olefins production ($mg \cdot g^{-1} \cdot h^{-1}$)
H−SSZ-13 (12C)	19.6	5.7	37.8	51.8	4.8	49.2	0.7	46.4
H−SSZ-13 (19C)	17.3	6.4	53.9	35.2	4.4	49.7	1.5	58.7
H−SSZ-13 (23C)	16.0	5.3	66.1	24.9	3.7	50.2	2.7	67.3
H−SSZ-13 (27C)	12.6	11.7	60.9	22.5	4.9	51.3	2.7	47.7
H−SSZ-13 (12S)	20.7	6.1	55.1	34.7	4.2	49.0	1.6	73.1
H−SSZ-13 (19S)	19.7	7.8	68.1	20.0	4.1	48.6	3.4	84.2
H−SSZ-13 (23S)	20.9	6.0	70.8	16.9	6.3	48.0	4.2	95.3
H−SSZ-13 (26S)	20.0	5.7	71.6	15.2	7.5	48.9	4.7	89.4

[a]Reduction condition: 583 K, atmospheric H_2, and GHSV = 6000 $mL \cdot g^{-1} \cdot h^{-1}$. Reaction condition: 653 K, 1.0 MPa, GHSV = 6000 $mL \cdot g^{-1} \cdot h^{-1}$, TOS = 800 min, $H_2/CO/N_2$ = 6/3/1, and OX/ZEO = 2.

12.6%. The poor activity should be put down to the large particle size of the zeolite which hindered the diffusion of the reactant and products.

The CO conversion over $ZnCrO_x$ + H−SSZ-13(S) during the STO reaction remained high no matter what Si/Al ratio H−SSZ-13(S) possessed. Light olefins in the hydrocarbon reached 70.8% at a CO conversion of 20.9% over the $ZnCrO_x$ + H−SSZ-13(23S) bifunctional catalyst at 653 K, 1.0 MPa, and GHSV = 6000 $mL \cdot g^{-1} \cdot h^{-1}$ after 800 min of reaction. The increase in CO conversion in the STO reaction via the OX−ZEO strategy was strongly associated with the thermodynamic driving force which originated from the rapid removal of methanol in the zeolite pores. The acid strength of H−SSZ-13(23S) was strong enough to ensure the high reactivity in the MTO reaction, thus promoting CO activation over $ZnCrO_x$. Meanwhile, the acid strength of H−SSZ-13(23S) was weak enough to prevent the excessive formation of paraffins from the hydrogenation of olefins, which would significantly change the product distribution. At last, the submicron H−SSZ-13 particles could facilitate the diffusion of reactants and products

https://doi.org/10.1021/acsomega.1c00751
ACS Omega 2021, 6, 10953−10962

and maintained high activity. Thus, the adequate acidic property and particle size of the zeolite were crucial to the catalytic performance of the STO reaction over the bifunctional catalyst. The particle size of H−SSZ-13 prepared by the conventional hydrothermal synthesis would increase inevitably, leading to the impairment of the catalytic performance along with the increase of the Si/Al ratio, which was essential to obtain the adequate acidic property. The seed-assisted hydrothermal synthesis could maintain the particle size of H−SSZ-13 at the submicron scale even at the high Si/Al ratio, thus producing H−SSZ-13 with both the adequate acidic property and the submicron particle size, leading to high CO conversion and light olefins selectivity at the same time during the STO reaction.

3. CONCLUSIONS

Submicron H−SSZ-13 with adequate acidic property was prepared by seed-assisted hydrothermal synthesis. The bifunctional catalyst containing H−SSZ-13 with a 100% H^+-exchanging degree was successfully utilized to produce light olefins from syngas. The adequate acidic property enabled the high light-olefins selectivity and CO conversion at the same time. The submicron particle facilitated the diffusion of the reactants and products, which provided a sustainable thermodynamic driving force between CO activation and C−C coupling, leading to high CO conversion. Light olefins in hydrocarbon reached 70.8% at a CO conversion of 20.9% over the $ZnCrO_x$ + H−SSZ-13(23S) bifunctional catalyst at 653 K, 1.0 MPa, and GHSV = 6000 $mL{\cdot}g^{-1}{\cdot}h^{-1}$ after 800 min of the STO reaction. By carrying out the MTO reaction under 0.6 MPa H_2 and 1.0 MPa syngas, the hydrogen transfer reaction was proved to have little impact on the high selectivity of paraffins during the STO reaction. The effect of H_2 over H−SSZ-13 on product distribution should be emphasized. Both CO and H_2 could alter the distribution of the retained carbonaceous species and the product during the MTO reaction, which influenced the light-olefins selectivity over the bifunctional catalyst in the STO process. This work revealed that CO and H_2 not only participated in CO activation over the metal oxide but also affected the C−C coupling in the zeolite pores, which provided new insight into the design of the bifunctional catalyst for the STO process via the OX−ZEO strategy.

4. EXPERIMENTAL SECTION

4.1. Synthesis of $ZnCrO_x$. $ZnCrO_x$ was prepared by the co-precipitation method based on our previous work.[4] $Zn(NO_3)_2{\cdot}6H_2O$ and $Cr(NO_3)_3{\cdot}9H_2O$ were dissolved in deionized water, and the Zn/Cr atomic ratio of the nitrate solution was 1. The nitrate solution was dropped into the $(NH_4)_2CO_3$ aqueous solution under stirring at 343 K until the pH value reached 7. After aging for 3 h, the suspension was washed and filtrated seven times. The residue was dried at 383 K overnight, followed by calcination at 773 K for 1 h.

4.2. Synthesis of Na−SSZ-13-Seed. The preparation of the Na−SSZ-13-seed was modified from the hydrothermal synthesis with a growth inhibitor discussed in our previous work.[35] Fumed silica and aluminum isopropoxide were utilized as the precursors of Si and Al, while *N*,*N*,*N*-trimethyl-1-adamant-ammonium hydroxide (25% TMAdOH) acted as the template. Anionic polyacrylamide (APAM, with a molecular weight of about 8 million) was used as the growth inhibitor. 0.85 g of NaOH was dissolved in 71.03 g of deionized water, followed by the slow addition of 2.67 g of aluminum isopropoxide under stirring. Then, 18.04 g of 25% TMAdOH was added dropwise into the gel. After 2-hour stirring, 6.41 g of fumed silica was added slowly and the gel was stirred for another 1 h. Then, 1.00 g of APAM was added, followed by stirring for 24 h. The gel was put in a 180 mL Teflon-lined stainless steel autoclave and kept at 433 K for 96 h under rotation. After crystallization, the samples were washed and centrifuged four times. After drying at 383 K overnight and following calcination at 823 K for 6 h under flowing air, the Na−SSZ-13-seed was gained.

4.3. Synthesis of H−SSZ-13(S). Submicron H−SSZ-13 was prepared by seed-assisted hydrothermal synthesis.[36] Silica sol (30% SiO_2) and $Al(OH)_3$ were utilized as the precursors of Si and Al, while *N*,*N*,*N*-trimethyl-1-adamant-ammonium hydroxide (25% TMAdOH) was the template. Na−SSZ-13-seed was used as the seed crystal. The gel was in the molar composition of $SiO_2/Al(OH)_3/TMAdOH/NaOH/H_2O$ = 100:*a*:20:20:4400, where "*a*" varied as the different Al content. The addition of the seed crystal was 1 wt % of the gel. First, NaOH was dissolved in deionized water, followed by the addition of $Al(OH)_3$. Then, 25% TMAdOH was added dropwise into the solution. After stirring for 30 min, 30% silica sol was added dropwise and kept stirring for 1 h. The Na−SSZ-13-seed was added at last, and the mixture was stirred for another 1 h. The gel was put in a 180 mL Teflon-lined stainless steel autoclave and kept at 433 K for 120 h under rotation. After crystallization, the samples were washed and centrifuged four times. The obtained sample was dried at 383 K overnight and calcined at 823 K for 6 h under flowing air. The calcined sample was ion-exchanged with 1 $mol{\cdot}L^{-1}$ NH_4Cl solution under 353 K for 2 h, and the ion exchange treatment was repeated three times. Then, the sample was washed and centrifuged three times. The obtained sample was dried at 383 K overnight and calcined at 823 K for 4 h under flowing air. The calcined sample was denoted as H−SSZ-13(*x*S), where "*x*" represents the molar ratio of Si/Al derived from ICP−OES, and "S" represents "seed-assisted".

4.4. Synthesis of H−SSZ-13(C). The conventional H−SSZ-13 was prepared by the hydrothermal synthesis procedure similar to the preparation of H−SSZ-13(S) but without the addition of seed crystal. Silica sol (30% SiO_2) and $Al(OH)_3$ were used as the precursors of Si and Al, while *N*,*N*,*N*-trimethyl-1-adamant-ammonium hydroxide (25% TMAdOH) was the template. The gel was in the molar composition of $SiO_2/Al(OH)_3/TMAdOH/NaOH/H_2O$ = 100:*b*:20:20:4400, where "*b*" varied as the different Al content. The detailed preparation procedure of H−SSZ-13(C) was almost the same as the procedure for H−SSZ-13(S) exceptthat there was no seed crystal addition. After the crystallization, washing, calcination, ion exchange treatment, washing, and calcination, the sample was obtained and denoted as H−SSZ-13(*y*C), where "*y*" represents the molar ratio of Si/Al derived from ICP−OES, and "C" represents "conventional".

4.5. Catalyst Characterization. X-ray powder diffraction (XRD) was carried out on a D/MAX 2550 VB/PC diffractometer. The X-ray source was Cu Kα radiation (40 kV and 100 mA).

ICP−OES was conducted on an Agilent 725 ICP−OES instrument. The samples were dissolved in hydrofluoric acid before the tests.

https://doi.org/10.1021/acsomega.1c00751
ACS Omega 2021, 6, 10953−10962

Scanning electron microscopy (SEM) tests were performed on a TESCAN MIRA3 scanning electron microscope.

Argon physisorption was performed on the Micromeritics ASAP 2020 surface area and porosity analyzer. The samples were degassed at 573 K for 10 h before the tests. Argon physisorption was carried out in a liquid argon bath. The liquid argon level was maintained by a polymer coating. The total surface area was evaluated by the BET equation. The external surface area and micropore area were calculated by the *t*-plot method.

NH_3−TPD measurements were carried out on the Micromeritics AutoChem II 2920 chemisorption analyzer. 100 mg of the sample was outgassed under 873 K for 1 h in flowing He. The adsorption of NH_3 proceeded in 10% NH_3/He for 30 min under 333 K. The excess NH_3 was purged by He for 30 min; then the thermal conductivity detector (TCD) signal was recorded as the temperature rising to 873 K with a heating rate of 10 K·min^{-1} in the flowing He.

Gas chromatography−mass spectrometry (GC−MS) tests were completed by the Agilent 7890A and Agilent 5975C GC−MS instrument with the HP-5 capillary column. The spent catalyst was dispersed in deionized water, followed by the addition of HF. The soluble carbonaceous species was extracted by CH_2Cl_2.

Thermogravimetric (TG) analysis was performed on the ThermoFisher Thermax 400 instrument from room temperature to 1173 K in 100 mL·min^{-1} air at the heating rate of 10 K·min^{-1}.

4.6. Catalytic Performance Test. Catalytic performance tests for the MTO process were carried out in a fixed-bed stainless steel reactor with quartz lining. H−SSZ-13 with the particle size of 250−425 μm was dried before being weighed. 200 mg of H−SSZ-13 was loaded in the reactor. The MTO reactions were carried out under different carrier gases. Generally, the sample was pretreated by the atmospheric carrier gas at 653 K for 120 min, then methanol was carried by the carrier gas to the reactor via a high-pressure low-temperature bubbler. The low-temperature bubbler ensured that the saturated methanol in carrier gas would not condense at room temperature. The temperature and pressure of the bubbler were determined by the Antoine equation of methanol. Considering the catalytic performance of $ZnCrO_x$ + H−SSZ-13, the feed of methanol was based on the condition of 20% CO conversion, 50% CO_2 selectivity, GHSV = 6000 mL·g^{-1}·h^{-1}, $H_2/CO/N_2$ = 60/30/10, and OX−ZEO = 2 in the STO reaction, which meant that the weight hourly space velocity (WHSV) of the methanol feed was 0.77 g·g^{-1}·h^{-1}. The detailed parameters of the bubbler and the reactor are listed in Table S1. The MTO reaction was carried out at 653 K for 800 min while the effluent was kept at 473 K and analyzed by an online Agilent 7890B GC with one TCD detector and two flame ionization detectors. Dimethyl ether was considered as the reactant in the calculation of methanol conversion.

Catalytic performance tests for the STO reaction were performed in a fixed-bed stainless steel reactor with quartz lining. $ZnCrO_x$ and H−SSZ-13 with the same particle size (250−425 μm) were dried before being weighed. 340 mg of $ZnCrO_x$ and 170 mg of H−SSZ-13 were mixed evenly before being loaded in the reactor. The catalytic performance was carried out at 653 K, 1.0 MPa, and GHSV = 6000 mL·g^{-1}·h^{-1} for 800 min after the reduction at 583 K for 180 min under atmospheric H_2. The composition of syngas was $H_2/CO/N_2$ = 60/30/10. An online Agilent 7890A GC was used to analyze the products. The carbon balance was higher than 98%.

The calculation of CO conversion was displayed as follows

$$X_{CO} = \frac{N_{CO,in} - N_{CO,out}}{N_{CO,in}} \times 100\% \quad (1)$$

where $N_{CO,in}$ and $N_{CO,out}$ refer to the molar flow of CO at the inlet and outlet, respectively.

The calculation of selectivity to CO_2 was displayed as follows.

$$S_{CO_2} = \frac{N_{CO_2,out}}{N_{CO,in} - N_{CO,out}} \times 100\% \quad (2)$$

where $N_{CO_2,out}$ refers to the molar flow of CO_2 at the outlet.

The calculation of hydrocarbon distribution of individual hydrocarbon C_iH_j was displayed as follows

$$S_{C_iH_j} = \frac{iN_{C_iH_j,out}}{\sum_{i=1}^{n} iN_{C_iH_j,out}} \times 100\% \quad (3)$$

where NC_iH_j,out refers to the molar flow of C_iH_j at the outlet.

■ ASSOCIATED CONTENT

Supporting Information

The Supporting Information is available free of charge at https://pubs.acs.org/doi/10.1021/acsomega.1c00751.

Detailed parameters of the catalytic performance test for the MTO processand textural properties of H−SSZ-13 (PDF)

■ AUTHOR INFORMATION

Corresponding Author

Weiyong Ying − *Engineering Research Center of Large Scale Reactor Engineering and Technology, Ministry of Education, State Key Laboratory of Chemical Engineering, School of Chemical Engineering, East China University of Science and Technology, Shanghai 200237, China;* orcid.org/0000-0003-3523-6702; Email: wying@ecust.edu.cn

Authors

Yuxuan Huang − *Engineering Research Center of Large Scale Reactor Engineering and Technology, Ministry of Education, State Key Laboratory of Chemical Engineering, School of Chemical Engineering, East China University of Science and Technology, Shanghai 200237, China*

Hongfang Ma − *Engineering Research Center of Large Scale Reactor Engineering and Technology, Ministry of Education, State Key Laboratory of Chemical Engineering, School of Chemical Engineering, East China University of Science and Technology, Shanghai 200237, China;* orcid.org/0000-0002-6752-9019

Zhiqiang Xu − *Engineering Research Center of Large Scale Reactor Engineering and Technology, Ministry of Education, State Key Laboratory of Chemical Engineering, School of Chemical Engineering, East China University of Science and Technology, Shanghai 200237, China*

Weixin Qian − *Engineering Research Center of Large Scale Reactor Engineering and Technology, Ministry of Education, State Key Laboratory of Chemical Engineering, School of Chemical Engineering, East China University of Science and*

Technology, Shanghai 200237, China; orcid.org/0000-0002-1049-9453

Haitao Zhang − *Engineering Research Center of Large Scale Reactor Engineering and Technology, Ministry of Education, State Key Laboratory of Chemical Engineering, School of Chemical Engineering, East China University of Science and Technology, Shanghai 200237, China;* orcid.org/0000-0002-1609-0501

Complete contact information is available at: https://pubs.acs.org/10.1021/acsomega.1c00751

Notes

The authors declare no competing financial interest.

■ ACKNOWLEDGMENTS

This work is supported by National High Technology Research and Development Plan of China (863 plan, no. 2011AA05A204).

■ REFERENCES

(1) Torres Galvis, H. M.; de Jong, K. P. Catalysts for Production of Lower Olefins from Synthesis Gas: A Review. *ACS Catal.* **2013**, *3*, 2130−2149.

(2) Goetze, J. *Operando Spectroscopy on the Reaction Mechanism and Deactivation of Methanol-to-Olefins Catalysts*; Utrecht University, 2018.

(3) Tan, L.; Wang, F.; Zhang, P.; Suzuki, Y.; Wu, Y.; Chen, J.; Yang, G.; Tsubaki, N. Design of the core-shell catalyst: an effective strategy for suppressing side reactions in syngas to light olefins direct selective conversion. *Chem. Sci.* **2020**, *11*, 4097−4105.

(4) Huang, Y.; Ma, H.; Xu, Z.; Qian, W.; Zhang, H.; Ying, W. Role of nanosized sheet-like SAPO-34 in bifunctional catalyst for syngas-to-olefins reaction. *Fuel* **2020**, *273*, 117771.

(5) Jiao, F.; Li, J.; Pan, X.; Xiao, J.; Li, H.; Ma, H.; Wei, M.; Pan, Y.; Zhou, Z.; Li, M.; Miao, S.; Li, J.; Zhu, Y.; Xiao, D.; He, T.; Yang, J.; Qi, F.; Fu, Q.; Bao, X. Selective conversion of syngas to light olefins. *Science* **2016**, *351*, 1065−1068.

(6) Jiao, F.; Pan, X.; Gong, K.; Chen, Y.; Li, G.; Bao, X. Shape-Selective Zeolites Promote Ethylene Formation from Syngas via a Ketene Intermediate. *Angew. Chem., Int. Ed.* **2018**, *57*, 4692−4696.

(7) Su, J.; Zhou, H.; Liu, S.; Wang, C.; Jiao, W.; Wang, Y.; Liu, C.; Ye, Y.; Zhang, L.; Zhao, Y.; Liu, H.; Wang, D.; Yang, W.; Xie, Z.; He, M. Syngas to light olefins conversion with high olefin/paraffin ratio using ZnCrOx/AlPO-18 bifunctional catalysts. *Nat. Commun.* **2019**, *10*, 1297.

(8) Cheng, K.; Gu, B.; Liu, X.; Kang, J.; Zhang, Q.; Wang, Y. Direct and Highly Selective Conversion of Synthesis Gas into Lower Olefins: Design of a Bifunctional Catalyst Combining Methanol Synthesis and Carbon−Carbon Coupling. *Angew. Chem., Int. Ed.* **2016**, *55*, 4725−4728.

(9) Ni, Y.; Liu, Y.; Chen, Z.; Yang, M.; Liu, H.; He, Y.; Fu, Y.; Zhu, W.; Liu, Z. Realizing and Recognizing Syngas-to-Olefins Reaction via a Dual-Bed Catalyst. *ACS Catal.* **2019**, *9*, 1026−1032.

(10) Li, N.; Jiao, F.; Pan, X.; Ding, Y.; Feng, J.; Bao, X. Size Effects of ZnO Nanoparticles in Bifunctional Catalysts for Selective Syngas Conversion. *ACS Catal.* **2019**, *9*, 960−966.

(11) Zhu, Y.; Pan, X.; Jiao, F.; Li, J.; Yang, J.; Ding, M.; Han, Y.; Liu, Z.; Bao, X. Role of Manganese Oxide in Syngas Conversion to Light Olefins. *ACS Catal.* **2017**, *7*, 2800−2804.

(12) Su, J.; Wang, D.; Wang, Y.; Zhou, H.; Liu, C.; Liu, S.; Wang, C.; Yang, W.; Xie, Z.; He, M. Direct Conversion of Syngas into Light Olefins over Zirconium-Doped Indium(III) Oxide and SAPO-34 Bifunctional Catalysts: Design of Oxide Component and Construction of Reaction Network. *ChemCatChem* **2018**, *10*, 1536−1541.

(13) Lok, B. M.; Messina, C. A.; Patton, R. L.; Gajek, R. T.; Cannan, T. R.; Flanigen, E. M. Silicoaluminophosphate molecular sieves: another new class of microporous crystalline inorganic solids. *J. Am. Chem. Soc.* **1984**, *106*, 6092−6093.

(14) Yang, G.; Wei, Y.; Xu, S.; Chen, J.; Li, J.; Liu, Z.; Yu, J.; Xu, R. Nanosize-Enhanced Lifetime of SAPO-34 Catalysts in Methanol-to-Olefin Reactions. *J. Phys. Chem. C* **2013**, *117*, 8214−8222.

(15) Song, W.; Fu, H.; Haw, J. F. Selective Synthesis of Methylnaphthalenes in HSAPO-34 Cages and Their Function as Reaction Centers in Methanol-to-Olefin Catalysis. *J. Phys. Chem. B* **2001**, *105*, 12839−12843.

(16) Olsbye, U.; Svelle, S.; Bjørgen, M.; Beato, P.; Janssens, T. V. W.; Joensen, F.; Bordiga, S.; Lillerud, K. P. Conversion of Methanol to Hydrocarbons: How Zeolite Cavity and Pore Size Controls Product Selectivity. *Angew. Chem., Int. Ed.* **2012**, *51*, 5810−5831.

(17) Liu, X.; Zhou, W.; Yang, Y.; Cheng, K.; Kang, J.; Zhang, L.; Zhang, G.; Min, X.; Zhang, Q.; Wang, Y. Design of efficient bifunctional catalysts for direct conversion of syngas into lower olefins via methanol/dimethyl ether intermediates. *Chem. Sci.* **2018**, *9*, 4708−4718.

(18) Wang, C.-M.; Wang, Y.-D.; Xie, Z.-K. Methylation of olefins with ketene in zeotypes and its implications for the direct conversion of syngas to light olefins: a periodic DFT study. *Catal. Sci. Technol.* **2016**, *6*, 6644−6649.

(19) Zhao, X.; Li, J.; Tian, P.; Wang, L.; Li, X.; Lin, S.; Guo, X.; Liu, Z. Achieving a Superlong Lifetime in the Zeolite-Catalyzed MTO Reaction under High Pressure: Synergistic Effect of Hydrogen and Water. *ACS Catal.* **2019**, *9*, 3017−3025.

(20) Zones, S. I. Zeolite SSZ-13 and its method of preparation. U.S. Patent US4544538A, 1985.

(21) Zhao, Z.; Yu, R.; Zhao, R.; Shi, C.; Gies, H.; Xiao, F.-S.; De Vos, D.; Yokoi, T.; Bao, X.; Kolb, U.; Feyen, M.; McGuire, R.; Maurer, S.; Moini, A.; Müller, U.; Zhang, W. Cu-exchanged Al-rich SSZ-13 zeolite from organotemplate-free synthesis as NH3-SCR catalyst: Effects of Na+ ions on the activity and hydrothermal stability. *Appl. Catal., B* **2017**, *217*, 421−428.

(22) Kwak, J. H.; Tonkyn, R. G.; Kim, D. H.; Szanyi, J.; Peden, C. H. F. Excellent activity and selectivity of Cu-SSZ-13 in the selective catalytic reduction of NOx with NH3. *J. Catal.* **2010**, *275*, 187−190.

(23) Fickel, D. W.; D'Addio, E.; Lauterbach, J. A.; Lobo, R. F. The ammonia selective catalytic reduction activity of copper-exchanged small-pore zeolites. *Appl. Catal., B* **2011**, *102*, 441−448.

(24) Wu, L.; Hensen, E. J. M. Comparison of mesoporous SSZ-13 and SAPO-34 zeolite catalysts for the methanol-to-olefins reaction. *Catal. Today* **2014**, *235*, 160−168.

(25) Wu, L.; Degirmenci, V.; Magusin, P. C. M. M.; Lousberg, N. J. H. G. M.; Hensen, E. J. M. Mesoporous SSZ-13 zeolite prepared by a dual-template method with improved performance in the methanol-to-olefins reaction. *J. Catal.* **2013**, *298*, 27−40.

(26) Wang, C.-M.; Wang, Y.-D.; Du, Y.-J.; Yang, G.; Xie, Z.-K. Similarities and differences between aromatic-based and olefin-based cycles in H-SAPO-34 and H-SSZ-13 for methanol-to-olefins conversion: insights from energetic span model. *Catal. Sci. Technol.* **2015**, *5*, 4354−4364.

(27) Müller, S.; Liu, Y.; Kirchberger, F. M.; Tonigold, M.; Sanchez-Sanchez, M.; Lercher, J. A. Hydrogen Transfer Pathways during Zeolite Catalyzed Methanol Conversion to Hydrocarbons. *J. Am. Chem. Soc.* **2016**, *138*, 15994−16003.

(28) Ilias, S.; Bhan, A. Mechanism of the Catalytic Conversion of Methanol to Hydrocarbons. *ACS Catal.* **2013**, *3*, 18−31.

(29) Kanai, J.; Martens, J. A.; Jacobs, P. A. On the nature of the active sites for ethylene hydrogenation in metal-free zeolites. *J. Catal.* **1992**, *133*, 527−543.

(30) Senger, S.; Radom, L. Zeolites as Transition-Metal-Free Hydrogenation Catalysts: A Theoretical Mechanistic Study. *J. Am. Chem. Soc.* **2000**, *122*, 2613−2620.

(31) Thommes, M.; Kaneko, K.; Neimark, A. V.; Olivier, J. P.; Rodriguez-Reinoso, F.; Rouquerol, J.; Sing, K. S. W. Physisorption of gases, with special reference to the evaluation of surface area and pore size distribution (IUPAC Technical Report). *Pure Appl. Chem.* **2015**, *87*, 1051−1069.

(32) Katada, N.; Igi, H.; Kim, J.-H. Determination of the Acidic Properties of Zeolite by Theoretical Analysis of Temperature-Programmed Desorption of Ammonia Based on Adsorption Equilibrium. *J. Phys. Chem. B* **1997**, *101*, 5969−5977.
(33) Hereijgers, B. P. C.; Bleken, F.; Nilsen, M. H.; Svelle, S.; Lillerud, K.-P.; Bjørgen, M.; Weckhuysen, B. M.; Olsbye, U. Product shape selectivity dominates the Methanol-to-Olefins (MTO) reaction over H-SAPO-34 catalysts. *J. Catal.* **2009**, *264*, 77−87.
(34) Mores, D.; Stavitski, E.; Kox, M. H. F.; Kornatowski, J.; Olsbye, U.; Weckhuysen, B. M. Space- and Time-Resolved In-situ Spectroscopy on the Coke Formation in Molecular Sieves: Methanol-to-Olefin Conversion over H-ZSM-5 and H-SAPO-34. *Chem.—Eur J.* **2008**, *14*, 11320−11327.
(35) Xu, Z.; Li, J.; Huang, Y.; Ma, H.; Qian, W.; Zhang, H.; Ying, W. Size control of SSZ-13 crystals with APAM and its influence on the coking behaviour during MTO reaction. *Catal. Sci. Technol.* **2019**, *9*, 2888−2897.
(36) Xu, Z.; Ma, H.; Huang, Y.; Qian, W.; Zhang, H.; Ying, W. Synthesis of Submicron SSZ-13 with Tunable Acidity by the Seed-Assisted Method and Its Performance and Coking Behavior in the MTO Reaction. *ACS Omega* **2020**, *5*, 24574−24583.

https://doi.org/10.1021/acsomega.1c00751
ACS Omega 2021, 6, 10953−10962